THE ASTROPHYSICAL JOURNAL, 292:22–28, 1985 May 1

AN [Fe x] λ6374 IMAGE OF PART OF THE CYGNUS LOOP

RICHARD G. TESKE AND ROBERT P. KIRSHNER
Department of Astronomy, The University of Michigan
Received 1984 September 14; accepted 1984 November 16

ABSTRACT

We have obtained an image of part of the Cygnus Loop in the [Fe x] λ6374 line at a resolution of 2".5, using a CCD preceded by an interference filter with a 9.5 Å bandpass. The data show a smooth intensity distribution associated with the supernova blast wave; superposed on this is a cloudlike surface-brightness pattern loosely associated with the optical nebulosity. The structures have properties consistent with evaporation of cloudlets into the blast wave interior.

Subject headings: nebulae: individual — nebulae: supernova remnants — shock waves

I. INTRODUCTION

In the analysis of soft X-ray observations of supernova remnants, it has often been the practice to determine from the X-ray data the best-fitting parameters for a Sedov spherical blast wave model (e.g., Kahn *et al.* 1980; Galas, Venkatesan, and Garmire 1981; Ku *et al.* 1984). Detection of the forbidden coronal radiation [Fe x] λ6374 and [Fe xiv] λ5303 from those remnants has generally been regarded as confirming a thermal origin for the X-rays and thus as supporting interpretation of the X-ray data in terms of a blast-wave model (Woodgate *et al.* 1974).

As observations of the forbidden coronal Fe lines have accumulated, it has become apparent that they cannot be entirely explained by the same models that satisfy the X-ray data (e.g., Lucke *et al.* 1980). The disagreement was underscored by nonequilibrium ionization models calculated by Teske (1984); agreement between modeled line intensities and observed intensities cannot be achieved in the context of the simple blast-wave model.

The basic idea of a thermal origin for the X-rays remains unquestioned. However, a second source mechanism for some of the forbidden iron emission, in addition to the blast wave, seems to be required. There is a consensus that the additional source probably has its origin in evaporative interactions between the shock front and cold cloudlets in the interstellar medium (McKee and Ostriker 1977). Such an interaction has been studied by Petre *et al.* (1982).

While the earlier published observations of the intensities of forbidden coronal iron lines (references cited by Teske 1984) have suggested the occurrence of cloudlet evaporation, those observations were made using wide apertures covering many arc minutes of sky, and they do not permit a clear test of the hypothesis. An adequate test of it requires data that can resolve structures of scale lengths typical for the process: a few 10^{17} cm and shorter. Thus real pictures made in the radiation of λ6374 and λ5303 are needed.

We are undetaking a program of observing portions of the Cygnus Loop and IC 443 in both of the coronal [Fe] lines at high angular resolution (2".5) on the sky. This paper describes some initial results from analysis of [Fe x] λ6374 images in the Cygnus Loop. The image shows the presence of a smooth brightness component associated with the blast wave, as well as a stronger, cloudlike surface brightness distribution behind the shock front which, according to our analysis, arises in evaporating cloudlets.

II. OBSERVATIONS

[Fe x] λ6374 images of portions of the Cygnus Loop were obtained at the 1.3 m McGraw-Hill telescope using the MASCOT CCD camera (Meyer and Ricker 1980) with an optical interference filter to isolate line radiation. The filter is well blocked to the wavelength limit of the CCD's sensitivity; its transmission of [O i] λ6364 light is negligible. The bandpass has a FWHM of 9.5 Å and a transmission "equivalent width" of 5.62 Å. In the direct mode the MASCOT instrument may be used as a reducing camera with a final f-ratio of f/1.5. The CCD as employed by us then provides a field of view of 8'.3 × 7'.1, each pixel subtending a square 2".5 on a side.

We measured the total efficiency of telescope and detector to be 13% at λ6374. Since the CCD readout noise is equivalent to 70 detected photons, several hours' exposure were necessary on each field to obtain a λ6374 image with adequate signal-to-noise ratio. Table 1 lists typical values for the photons actually collected in a single observation.

Subtraction of bias frames and dark exposure frames is a potential source of additional noise which must be suppressed. The bias frames were fitted by a parabolic surface using least squares, and this smooth surface was subtracted from the data

TABLE 1

PHOTON STATISTICS FOR A CYGNUS OBSERVATION[a]

Object	Measured Intensity Level (ergs cm^{-2} s^{-1} sr^{-1})	Number of Detected Photons in a Pixel
Sky background	22.7×10^{-7}	1270
NGC 6995 (bright)	7×10^{-7}	393
NGC 6995 (faint)	2×10^{-7}	112

[a] Each exposure 10,800 s.

frames. Three 3 hr dark frames were bias-subtracted in the same fashion and then simply averaged before being applied to the data frames. As a result, the typical noise contributions are as follows (N is a number of detected photons):

$$(\sigma^2)_{\rm data} = N_{\rm nebula} + N_{\rm sky} + N_{\rm dark\ frame} + (N^2)_{\rm read\text{-}out}$$

$$(\sigma^2)_{\rm data} = 112 + 1270 + 1010 + 4800$$

Clearly, CCD readout noise is the major noise source in the data reported here. Its reduction to 10 electrons or less would eliminate it as a problem in such observations. Buildup of dark charge is also obviously important, but is manageable.

Spectrophotometric standards, which were observed each night, were taken from the list of stars calibrated by Cochran (1981). On the first night, six exposures of four stars were made, two at the beginning, two at the middle, and two at the end of the night, covering an airmass range of 1.23 to 1.44. In terms of flat-fielded picture unit (PU) values, the calculated energies deposited ranged from 3.28×10^{-11} to 3.67×10^{-11} ergs PU^{-1} cm^{-2} of the telescope primary mirror, with averages at the beginning, middle, and end of the night being 3.58, 3.54, and 3.38×10^{-11} ergs PU^{-1} cm^{-2}. Thus there was a slow but tolerable drift of sky transparency. On the second observing night, five observations of the four stars yielded closely similar results. Each night's calibrations had an internal rms error of 1.5%. Since the final mean values for each night ($3.50 \pm 0.052 \times 10^{-11}$ and $3.37 \pm 0.049 \times 10^{-11}$ ergs PU^{-1} cm^{-2}) were closely the same, and since only small variations in sky transparency took place during the course of each night, we believe that our photometric calibrations are reliable to better than 20%, and are probably reliable to better than 10%.

Two 3 hr exposures of the southern portion of NGC 6995 in the Cygnus Loop were added together to obtain the [Fe x] image discussed in the next section. The map has a resolution of 2".5 per pixel. The noise in a picture element is $\pm 1.4 \times 10^{-7}$ ergs cm^{-2} s^{-1} sr^{-1}. This estimate includes CCD readout noise and the square root of the detected number of photons from skyglow and nebula.

Individual stars were removed from the image frames before the frames were combined. A two-dimensional parabolic surface was locally fitted by least squares to the background signal in pixels surrounding each star image, and the signal values in each pixel containing a star were replaced by the corresponding value from the mean background surface that had been fitted. This process tends to leave visible "scars" in locations where star images covered many picture elements. The method does not remove the background signal contributed by faint starlight. This weak contribution to the sky brightness is eliminated, on the average, upon later subtraction of a value for the night sky, but statistical fluctuations in the faint starlight remain as a source of noise. We estimate this to be less than $\pm 1 \times 10^{-7}$ ergs cm^{-2} s^{-1} sr^{-1}.

Figure 1 shows the final, processed CCD image of NGC 6995. The λ6374 emission nebulosity appears as a dark structure on the right side of the frame. The feature at the extreme lower left corner is an artifact introduced by flattening problems. In Figure 1 the darkest features correspond with intensities brighter than 10×10^{-7} ergs cm^{-2} s^{-1} sr^{-1}, while the lightest tones refer to *negative* intensities $< -5 \times 10^{-7}$ ergs cm^{-2} s^{-1} sr^{-1}, below the mean sky level of zero.

III. RESULTS

The λ6374 image of NGC 6995 shows surface brightness variations of small spatial scale. There are significant intensity fluctuations on a scale from around 1' down to 10" (0.04 pc). For example, in the lower right of Figure 1 a patch of nebulosity roughly 25 pixels on a side shows brightness fluctuations ΔI_λ in excess of 2×10^{-7} ergs cm^{-2} s^{-1} sr^{-1} on a scale of 3 or 4 pixels.

a) NGC 6995

The location of our Cygnus Loop image is at the southern end of NGC 6995, at the position of strongest soft X-ray emission shown in the *Einstein* IPC picture (Ku *et al.* 1984). The region lies just to the south of the filament analyzed by Hester, Parker, and Dufour (1983).

In Figure 2 we show the contour map of [Fe x] intensity superposed on a copy of the POSS red print. The map has been smoothed to 7".5 × 7".5 resolution to improve the signal-to-noise ratio. While there is a general spatial correspondence between source regions of λ6374 radiation and regions of warm optical filaments emitting Hα + [N II] + [S II], the correspondence is not exact and the detailed surface brightness maps are markedly different. The regions of brightest [Fe x] are clearly associated with some of the warm optical filaments; on the other hand, large areas of the warm filaments have only weak [Fe x] associated with them.

It is possible that a part of the surface brightness seen in the map is due to contamination by Paschen continuum radiation from the warm optical filaments. We can estimate that contribution using the Hβ fluxes measured in the Cygnus Loop by Fesen, Blair, and Kirshner (1982). At their position *Y*—a considerably brighter filament than those seen at the location of the nebulosity in Figure 2—they measured an Hβ flux of 7.7×10^{-14} ergs cm^{-2} s^{-1} within their aperture of 2".8 × 40". Hester, Parker, and Dufour (1983) have shown that Hα (and so presumably Hβ) intensity variations correlate well with the [N II] intensities. Thus we have used the [N II] temperature of 11,000 K at position *Y* determined by Fesen, Blair, and Kirshner (1983) together with their Hβ flux to calculate the expected Paschen continuum signal in our λ6374 bandpass. Emissivities were taken from Osterbrock (1974). No reddening correction was applied. We calculate that the continuum signal averaged over an area of 2".8 × 40" should be no greater than 1.1×10^{-7} ergs cm^{-2} s^{-1} sr^{-1}.

The continuum signal will be clumpy and similar in overall appearance to the warm optical filaments. We currently have no way of knowing what its peak intensities will be, but for two reasons believe that the continuum intensity has not greatly distorted the information in the λ6374 line. First, to judge from red photographs of the region, the Hβ flux that was used in the above calculation is larger than would actually be measured at the location of the emission in Figure 2, so that the real averaged intensity is lower than our estimate. Second, the spatial distribution of λ6374 intensity in Figure 2 is clearly different from the optical nebulosity, and the peak iron brightness is located on a region of fairly faint filaments. Thus the λ6374 emission is likely to be well portrayed by our image in NGC 6995.

According to the *Einstein* X-ray data discussed by Ku *et al.* (1984), the edge of the X-ray emission in our field of view lies nearly north-south on the sky. We have assumed that the X-rays display the location of the shock front. In making our observations we attempted to place the shock front at the center of the CCD frame; as a result the [Fe x] emission knots are crowded to the right edge of the field. This has, however, enabled us to determine a reliable value of the night-sky bright-

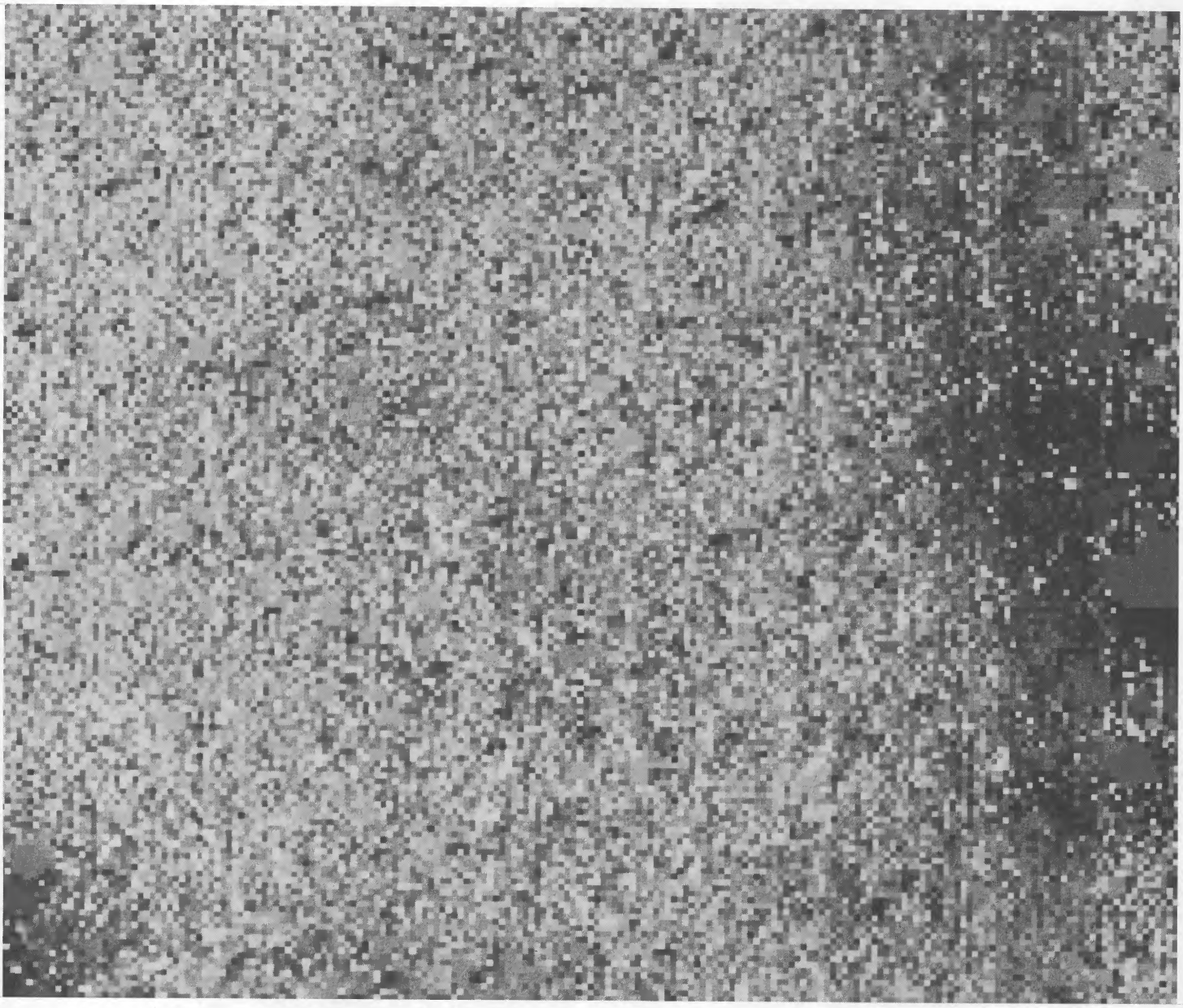

FIG. 1.—This processed CCD image of NGC 6995 is printed as a negative and shows the λ6374 emission as a dark feature on the right. Each pixel is 2.″5 on a side; the frame size is 8.′3 × 7.′1. Darkest tones: $I_\lambda \geq 10 \times 10^{-7}$ ergs cm^{-2} s^{-1} sr^{-1}. Lightest tones: $I_\lambda \leq -5 \times 10^{-7}$ ergs cm^{-2} s^{-1} sr^{-1} (below mean sky).

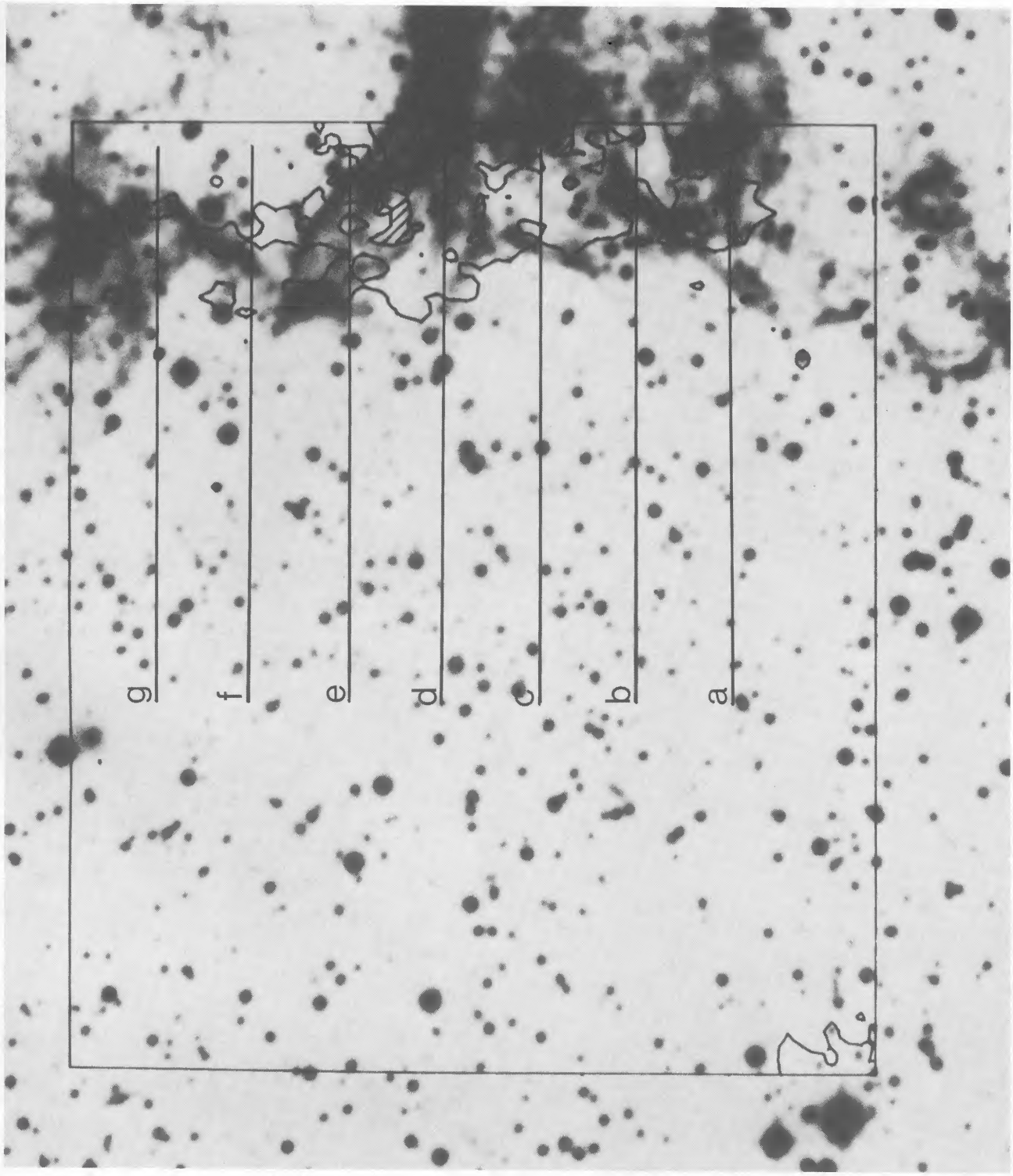

FIG. 2.—Contours of [Fe x] λ6374 intensity in NGC 6995 are here superposed on a copy from the POSS red print. The contour levels are 5 and 10 (*cross-hatched*) $\times 10^{-7}$ ergs cm^{-2} s^{-1} sr^{-1}. The dark lines *a* through *g* show the central trace of each of the profiles in Fig. 3.

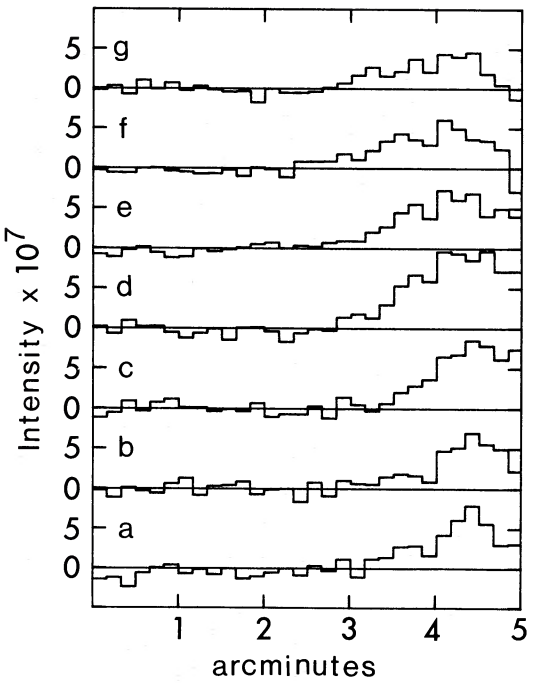

FIG. 3.—Profiles of average intensity of the λ6374 line perpendicular to the shock front. The intensity is given in units of ergs cm^{-2} s^{-1} sr^{-1}. The location on the sky of these profiles is depicted in Fig. 2.

ness from the eastern half of the image. The measured value—which has been subtracted to yield the contours of Figure 2—is 22.6×10^{-7} ergs cm^{-2} s^{-1} sr^{-1} after elimination of brighter individual stars, and is in good agreement with the predicted value of 24.5×10^{-7}, which is composed of airglow (15.2×10^{-7}, Broadfoot and Kendall 1972) and galactic starlight (9.3×10^{-7} at latitude $b = 10°$, Roach and Megill 1961).

To explore the structure of the shock front we have generated seven east-west intensity profiles, which are shown as histograms in Figure 3. In the profiles each histogram bar represents the average intensity in a rectangle 21 × 4 pixels; the long dimension of the 52.″7 × 10.″0 rectangle is oriented north-south, parallel to the shock front. The central trace of each scan line is depicted in Figure 2.

The profiles show a gradual increase of [Fe x] intensity beginning near the middle of each; the origin of the rise places the location of the intercloud shock front roughtly 2′ east of the Hα + [N II] + [S II] nebulosity. This is close to the edge of the soft X-ray emission (Ku *et al.* 1984) and thus confirms the thermal nature of the X-rays at the shock front. Behind the shock the λ6374 intensity rises slowly to $2–3 \times 10^{-7}$ ergs cm^{-2} s^{-1} sr^{-1} within the first 1.′5 to 2′, followed by a stronger, abrupt rise near the edge of the warm optical filaments. For a distance to NGC 6995 of 770 pc, and for a remnant radius of 20 pc, the arc-distance of 1.′5–2′ corresponds with $R/R_{\rm shock} = 0.015–0.02$.

Our profiles are qualitatively similar to [Fe x] and [Fe XIV] profiles obtained at much lower resolution in NGC 6992 by Lucke *et al.* (1980). Their data also show a weak intensity rise a few arc minutes outside the warm optical filaments and an abrupt intensity increase at the filament positions. However, the λ6374 intensities at the location observed by us are up to 10 times greater than the intensities quoted by them. This discrepancy is likely due to clumping of λ6374 emission on the small spatial scales which are resolved in the CCD image.

The observed smooth rise of λ6374 intensity behind the shock may be compared with the modeled brightness distributions (Teske 1984) for spherical blast waves. According to the models, an intensity rise like that seen here is consistent with a shock of speed $V_s = 250–300$ km s^{-1} propagating into a cold medium with ambient particle density $n_0 = 0.5–1$ cm^{-3}. These values are in good agreement with parameters obtained by Woodgate, Kirshner, and Balon (1977) and by Touhy, Nousek, and Garmire (1979) for a location in NGC 6992 some 35′ north of the region studied here, and they disagree with parameters relevant to the Sedov model of the Cygnus Loop as a whole (Ku *et al.* 1984). This reflects a local difference in the structure of the shocked interstellar medium near NGC 6992–6995, compared with the large-scale structure typical of the remnant as a whole, as Ku *et al.* (1984) have pointed out.

In the vicinity of the warm optical filaments, the intensity of λ6374 emission is significantly enhanced; the map shows that there the million-degree gas breaks up into a patchy, cloudlike structure. According to the scheme of a three-phase interstellar medium (McKee and Ostriker 1977), the hot gas has had its origin in cold, neutral cloudlets which have been overtaken and enveloped by the expanding supernova blast wave. When it encounters a cloud, the blast wave drives a slower shock into the cloud; later the cloud will tend to evaporate into the surrounding low-density plasma of the remnant's interior (Cowie and McKee 1977). Within the shocked cloudlets, higher densities and lower postshock temperatures shorten the radiative cooling time of the shocked gas, giving rise to small, optically bright source regions behind the shock front; these volumes are the warm optical filaments (Cox 1972; Raymond 1979; Fesen, Blair, and Kirshner 1982). Support for the evaporative cloudlet–shock interaction has been presented by Petre *et al.* (1982), who discussed high-resolution X-ray observations of Pup A and concluded that soft X-ray and [Fe XIV] λ5303 emission from a knot on the northeastern rim of that remnant arises in a hot envelope associated with a recently shocked, evaporating coudlet of mass $1.4\ M_\odot$.

As shown below, we have tested the idea that the bright [Fe x] condensations observed by us in NGC 6995 are also cloudlets evaporating into the interior of the Cygnus blast wave, and have concluded that our data support the general hypothesis described above as well.

b) Evidence for Evaporation in NGC 6995

The first evidence we have is that the evaporative time scale for the condensations/cloudlets exceeds the time that has elapsed since they were engulfed by the blast wave. Since the condensations lie roughly $2' = 1.4 \times 10^{18}$ cm behind the shock, which has a speed $V_s = 250–300$ km s^{-1}, the shock passed them by approximately 1500–1800 yr ago, assuming they were not accelerated in the encounter. The characteristic evaporation time for a cloud immersed in a surrounding plasma of electron temperature T_f is given by Cowie and McKee (1977):

$$t_{\rm evap} = 3.3 \times 10^{20} n_c (R_c)^2 (T_f)^{-5/2} \ln \Lambda / 30 \text{ yr}, \quad (1)$$

where n_c = mean hydrogen density in the cloud and R_c is its radius in parsecs. The Coulomb logarithm $\ln \Lambda$ is to be evaluated for temperature T_f and density n_f in the surrounding plasma. From our blast wave models (Teske 1984) with $V_s = 250–300$ km s^{-1}, and at a distance of $R/R_{\rm shock} = 0.02$ behind

the front, we adopt $T_f = 0.9$–1.3×10^6 K, $n_f = 2.0$–3.8 cm^{-3}. The observed [Fe X] condensations have sizes in the range 30″ to 60″, so that $R_c = 0.06$–0.12 pc. If typical cloudlet densities are in the range 10–100 cm^{-3}, then their minimum characteristic evaporation time of 6100 yr calculated from equation (1) exceeds their immersion time by nearly a factor of 4 in NGC 6995. It is then reasonable to expect that we might be observing the evaporation process today.

The time needed for the process to establish a state of steady flow was approximately calculated by Cowie and McKee (1977) to be

$$t_{\rm flow} = 4.2 \times 10^{25} R_c{}^3 n_f/\dot{m} \text{ yr} , \quad (2)$$

where $\dot{m}$ is the rate of mass loss. Using a rate of 7×10^{18} g s^{-1}, which we calculate below, we find

$$2500 < t_{\rm flow} < 39{,}000 \text{ yr} ;$$

this result suggests that if cloud evaporation is being observed, then the process has probably not yet reached a steady state in NGC 6995.

The values of T_f, n_f, and R_c deduced above from the observations and models support the hypothesis that we are observing an evaporative flow rather than a condensing one. This will be true if the radiative cooling time of the intercloud gas is much greater than the evaporation time for a cloud. With

$$t_{\rm cooling} = kT_f/n_f\Lambda(T_f) \text{ s} ,$$

and with a value for the radiative loss rate $\Lambda(T)$ taken from Rosner, Tucker, and Vaiana (1978) ($\log \Lambda(T_f) = -21.94$), we compute

$$9000 < t_{\rm cooling} < 25{,}000 \text{ yr} .$$

Thus the cooling time exceeds the minimum characteristic evaporation time for a cloud, but only by a small factor, suggesting that conductive heating is just marginally more important than radiative cooling.

McKee and Cowie (1977) analytically estimated the critical cloud radius $R_{\rm rad}$ below which clouds evaporate, and above which the intercloud medium condenses onto them:

$$R_{\rm rad} = 4.8 \times 10^5 T_f{}^2/n_f \text{ cm} .$$

For the range of temperature and density estimated above, we have $0.03 < R_{\rm rad} < 0.13$ pc, to be compared with the observed radius range $0.06 < R_c < 0.12$ pc. Again it seems that if conductive heating does win out over radiative cooling, it does so by a small margin. A clear-cut decision can be made through more exact determination of T_f and n_f in the postshock gas, and by obtaining less noisy λ6374 images that will allow a more certain measurement of the cloud radii.

Since the minimum cooling time (9000 yr) for the intercloud gas greatly exceeds the estimated maximum immersion time of the clouds (1800 yr), there has not been time to establish a bright and dense cooling flow. We therefore think that cloud heating tends to predominate, and that we are observing evaporation in NGC 6995.

A second piece of evidence favoring the evaporation interpretation of the data is that the mass of [Fe X] gas in the area observed is roughly the same (within a small factor) as the mass expected to have been lost from cloudlets at the same location. We estimate the masses as follows.

The rate of evaporation of a cloudlet is regulated by thermal conduction of energy into it from the surrounding plasma. Cowie and McKee (1977) investigated the evaporation of spherical clouds when the ambient particle density is so low that the mean free path of electrons—which chiefly conduct the heat energy—exceeds the temperature scale height in the cloud vicinity. Under that extreme condition the heat flux q is no longer proportional to grad T, but rather depends on $n_e(T_e)^{3/2}$. They refer to the effect as *saturation*, and write the saturated heat flux as $q_{\rm sat} = 5\phi_s \rho c^3$, where $c^2 = kT/\mu$ and ϕ_s is a factor of order unity.

Whether the classical heat flux exceeds the saturated heat flux may be judged from the numerical value of a parameter σ_0 (Cowie and McKee 1977). For $\sigma_0 > 1$, the heat flux is saturated. In general, $\sigma_0 \ll 1$ in the interior of a supernova blast wave; in particular, for NGC 6995 we find $\sigma_0 < 0.4$, so that clouds enveloped by the shock front may be considered to be heated by classical thermal conduction.

The rate of mass loss for steady flow in the classical case is given by Cowie and McKee (1977) as

$$\dot{m}_{\rm classical} = 2.68 \times 10^{11} \mu R T_f{}^{5/2}/\ln \Lambda \text{ g s}^{-1} , \quad (3)$$

where R is in cm. Hence the mass-loss rate from a single cloud in NGC 6995 is

$$2.3 \times 10^{18} < \dot{m}_{\rm classical} < 1.2 \times 10^{19} \text{ g s}^{-1} ,$$

depending on the choice of cloud radius and T_f. This calculation assumes that steady evaporation has been established, a condition that is probably not realized, as we have seen. Nevertheless we use it to estimate the amount of material that may have been evaporatively added to the interior of the shock wave in Cygnus.

To estimate the total amount of mass loss in the observed part of the nebula we have to guess the number of cloudlets there. Several are definitely seen in our map; there may be around a dozen altogether. We therefore suppose for the calculation that there may be the remains of 10 clouds in the brightest portion of the [Fe X] map. With $\dot{m} = 7 \times 10^{18}$ g s^{-1} and $\Delta t = 5 \times 10^{10}$ s, we get

$$M = N_{\rm clouds} \dot{m} \Delta t = 0.002 \, M_\odot ,$$

approximately. This is the mass of gas added to the blast wave by evaporation near the warm optical filaments in the field of view.

This mass may be compared with the mass of gas emitting the red λ6374 line if the line emissivity is known; we will adopt an equilibrium calculation. In earlier modeling work (Teske 1984), it was shown that for a shock speed $V_s < 300$ km s^{-1} (the case here) both $T_{\rm ion}$ and $T_{\rm electron}$ will remain close to one another behind the shock, and that ionization conditions will remain fairly close to their equilibrium values. Because electrons are the agents of both heat conduction and ionization in the evaporation process, it is reasonable to expect that collisional ionization and excitation proceed roughly at their equilibrium rates. Thus it is useful to employ an emissivity for the equilibrium case.

Further, at the shock speed $V_s = 250$–300 km s^{-1}, the gas is evaporating into a medium whose temperature is close to the value at which Fe^{+9} reaches its maximum ionic concentration.

Thus we write, for the equilibrium case and for an iron abundance $\log A = 7.4$,

$$(I_{\lambda 6374})_{\rm obs} = 1/4\pi \int \rho \epsilon dy$$
$$= 1.02 \times 10^{-26} \int n_e{}^2 dy \quad (4)$$

ergs cm^{-2} s^{-1} sr^{-1}. We will assume uniform conditions of temperature and density along a line of sight whose path length is Y cm, and across an area on the nebula of A cm^2. Thus the mean square electron density is

$$\langle n_e^2 \rangle = 9.8 \times 10^{25} I_\lambda / Y \text{ cm}^{-6} ,$$

and the total mass of emitting gas is

$$M = \rho V = \rho A Y = 1.9 \times 10^{-11} A (Y I_\lambda)^{1/2} \text{ gm} ,$$

where we have assumed that $n_e = n_H + 2n_{He} = 1.09n$.

The average brightness of the [Fe X] knots over and above the blast wave background of 3×10^{-7} ergs cm^{-2} s^{-1} sr^{-1} is measured to be nearly 3×10^{-7} ergs cm^{-2} s^{-1} sr^{-1} within a region of the image corresponding with a projected area of $A = 1.7 \times 10^{36}$ cm^2. We assume that the thickness of the emitting volume along the line of sight is $Y_{pc} = 2R_c$, using for R_c the values assigned earlier.

We therefore obtain a mean electron density n_e of 6–10 cm^{-3}, comparable with the value of 12 cm^{-3} got by Petre *et al.* (1982) for the evaporating knot in Pup A.

The minimum mass of the gas which emits λ6374 in our field of view, in excess of that contained by the intercloud shock wave, is

$$0.005 < M < 0.007 \, M_\odot .$$

This value is in fair agreement with our prior estimate of 0.002 $M_\odot$ which could have been evaporated since the time the cold condensations were first enveloped by the shock. Considering the crudeness of both calculations, the agreement of the results can be taken as supporting the notion that our λ6374 observations portray the evaporation of material in NGC 6995.

A third piece of evidence in support of the evaporative hypothesis is balance between the pressure of the [Fe X] evaporata and pressure in the blast wave itself. With $n = (1.1/1.2)n_e$, and $(n_e)_{\text{evaporata}} = 10$ cm^{-3}, $(n)_{\text{blast wave}} = 2$ to 3.8 cm^{-3},

$$(p_{\text{evaporata}})/(p_{\text{blast wave}}) = 2.4\text{–}4.5 .$$

The approximate equality suggests that there does indeed exist a near pressure balance. If we take these very rough numbers at face value, they may indicate an overpressure in the evaporative flow relative to the ambient intercloud medium, a condition also found by Petre *et al.* (1982), and one that would be expected in the case of supersonic flow (Cowie and McKee 1977).

Our quantitative inferences from the data endorse the evaporative hypothesis and thus explain in a *general* way why bright knots of λ6374 emission are found in the vicinity of the warm optical filaments. But the significant differences (see Fig. 2) in the *detailed* surface brightness distributions of [Fe X] and Hα + [N II] + [S II] are yet to be addressed. These differences may reflect variations in cloudlet mass-loss rate, differences in total mass lost, unusual structure in the evaporative flow, and so on, variations which can be traced to the likely existence of a mixture of cloud sizes, masses, and densities. Further observations in [Fe XIV] are planned, together with detailed numerical modeling of cloud evaporation, in the expectation that these efforts will help to unravel the complex processes which are taking place at the southern tip of NGC 6995.

IV. SUMMARY

[Fe X] λ6374 images resolving 2".5 have been obtained on a portion of NGC 6995 in the Cygnus Loop. The data show the presence of cloudlets or condensations on scales 30" to 60"; when the image is smoothed to a resolution of 7".5, structure down to 10" is clearly seen in the larger features.

The Cygnus data point to the present location of the supernova blast wave front as being about 2' east of the Hα + [N II] + [S II] warm optical filaments in the region, in accord with the soft X-ray data (Ku *et al.* 1984). Profiles of the [Fe X] intensity behind the shock front are consistent with a shock speed of $V_s = 250$–300 km s^{-1} and a preshock particle density of $n_0 = 0.5$–1 cm^{-3}.

Existing in association with the warm optical filaments in NGC 6995 is a patchy or cloudlike [Fe X] emission nebulosity. We have interpreted the structures there as being principally the result of evaporation of shocked cloudlets into the interior of the blast wave, basing the conclusion upon the rough agreement between the amount of gas we calculate to have been evaporatively evolved and the amount of gas presently emitting the λ6374 line in the nebulosity. Our data thus offer further support for the hypothesis that evaporation of shocked cloudlets in the interior of a blast wave is an important process contributing to the overall structure of the interstellar medium (Petre *et al.* 1982).

In selecting the region to be observed in Cygnus we were guided by the *Einstein* X-ray map. We thank Dr. William Hsin-Min Ku for communicating it prior to publication. We especially thank Drs. George Ricker and John Doty for their generous assistance in preparing the MASCOT instrument and for instruction in its use. To Mr. Greg Aldering go thanks for translating magnetic tapes. Work supported in part by NSF grant AST 83-09496.

REFERENCES

Broadfoot, A. L., and Kendall, K. R. 1972, *J. Geophys. Res.*, **73**, 426.
Cochran, A. L. 1981, *Ap. J. Suppl.*, **45**, 83.
Cowie, L. L., and McKee, C. F. 1977, *Ap. J.*, **211**, 135.
Cox, D. P. 1972, *Ap. J.*, **178**, 143.
Fesen, R. A., Blair, W. P., and Kirshner, R. P. 1982, *Ap. J.*, **262**, 171.
Galas, C. M. F., Venkatesan, D., and Garmire, G. P. 1981, *Ap. J.*, **250**, 216.
Hester, J. J., Parker, R. A. R., and Dufour, R. J. 1983, *Ap. J.*, **273**, 219.
Kahn, S. M., Charles, P. A., Bowyer, S., and Blissett, R. J. 1980, *Ap. J.* (*Letters*), **242**, L19.
Ku, W. H.-M., Kahn, S. M., Pisarski, R., and Long, K. S. 1984, *Ap. J.*, **278**, 615.
Lucke, R. L., Woodgate, B. E., Gull, T. R., and Socker, D. G. 1980, *Ap. J.*, **235**, 882.
McKee, C. F., and Cowie, L. L. 1977, *Ap. J.*, **215**, 213.
McKee, C. F., and Ostriker, J. P. 1977, *Ap. J.*, **218**, 148.
Meyer, S. S., and Ricker, G. R. 1980, *S.P.I.E. Proc., No. 264, Applications of Digital Imaging to Astronomy*, p. 38.
Osterbrock, D. E. 1974, *Astrophysics of Gaseous Nebulae* (San Francisco: W. H. Freeman).
Petre, R., Canizares, C. R., Kriss, G. A., and Winkler, P. F., Jr. 1982, *Ap. J.*, **258**, 22.
Roach, F. E., and Megill, L. R. 1961, *Ap. J.*, **133**, 228.
Rosner, R., Tucker, W. H., and Vaiana, G. S. 1978, *Ap. J.*, **220**, 643.
Teske, R. G. 1984, *Ap. J.*, **277**, 832.
Tuohy, I. R., Nousek, J. A., and Garmire, G. P. 1979, *Ap. J.* (*Letters*), **234**, L101.
Woodgate, B. E., Stockman, H. S., Jr., Angel, J. R. P., and Kirshner, R. P. 1974, *Ap. J.* (*Letters*), **188**, L79.
Woodgate, B. E., Kirshner, R. P., and Balon, R. J. 1977, *Ap. J.* (*Letters*), **218**, L129.

ROBERT P. KIRSHNER and RICHARD G. TESKE: Department of Astronomy, The University of Michigan, Ann Arbor, MI 48109